# 3D Solution Structure of [Tyr$^3$]Octreotate Derivatives in DMSO: Structure Differentiation of Peptide Core Due to Chelate Group Attachment and Biologically Active Conformation#

G. A. Spyroulias*,[1], A. S. Galanis[1], Ch. Petrou[1], D. Vahliotis[2], P. Sotiriou[1], A. Nikolopoulou[3], B. Nock[3], T. Maina[3] and P. Cordopatis*,[1]

[1]*Department of Pharmacy, University of Patras, GR-26504, Patras Greece;* [2]*Center of Instrumental Analysis, University of Patras, GR-26504, Patras, Greece;* [3]*Institute of Radioisotopes-Radiodiagnostic Products, NCSR "Demokritos", GR-15310 Athens, Greece*

**Abstract:** The solution models of [Tyr$^3$]octreotate (DPhe$^1$-Cys$^2$-Tyr$^3$-DTrp$^4$-Lys$^5$-Thr$^6$-Cys$^7$-Thr$^8$-COOH, disulfide bridged) **(I)**, its analogs functionalized with an open chain tetraamine chelator, $N_4$-[Tyr$^3$]octreotate **(II)**, and the $N_4$-$(Asp)_2$-[Tyr$^3$]octreotate **(III)** peptide have been determined through 2D $^1$H NMR spectroscopy in DMSO. Chemical shift analysis has been performed in an attempt to elucidate structural changes occurring during attachment of the tetraamine to the peptide backbone. NMR-derived geometrical constraints have been used in order to calculate high resolution conformers of the above peptides. Conformational analysis of the three synthetic analogues, have shown that these somatostatin analoges adopt a predominant antiparallel $\beta$-sheet conformation characterized by a $\beta$-like turn spanning residues DTrp$^4$ and Lys$^5$ which is supported in the case of $N_4$-$(Asp)_2$-[Tyr$^3$]octreotate and $N_4$-[Tyr$^3$]octreotate by medium range NOEs. These data indicate that the above-mentioned molecules adopt a rather constrained structure in the 4-residue loop Tyr$^3$-Thr$^6$. Additionally, the C-terminal of [Tyr$^3$]octreotate, comprising Cys$^7$ and Thr$^8$, appears to form a turn-like structure manifested by characteristic side-chain NOEs between Lys$^5$ and Thr$^8$, which have not been detected for the other two compounds. These data are discussed in the light of previous structural data of Sandostatin (octreotide) and suggest that attachment of the $N_4$-chelator and two Asp residues at the N-end of [Tyr$^3$]octreotate impose considerable structural changes and affect the binding properties of these peptides. Indeed, the $IC_{50}$ values determined during competition binding assays against the $sst_2$ (somatostatin subtype 2 receptor) suggest that the presence of the $N_4$ group enhances receptor affinity, while extension of peptide chain by two negatively-charged Asp residues impairs receptor affinity at approximately one order of magnitude.

**Keywords:** Somatostatin analogues, Sandostatin, octreotate, Demotate, NMR Conformational Analysis.

***#This article is dedicated to the memory of Prof Murray Goodman for his scientific contributions to peptide science and for his enthusiastic promotion of peptide science.***

## INTRODUCTION

Somatostatin, a cyclic tetradecapeptide also known as somatotropin release inhibiting factor (SRIF), plays a prominent role in the regulation of various functions in several human tissues [1]. Among the key actions of somatostatin one should note the control of hormone release, mainly of growth hormone, glucagon or insulin, from its target cells [2,3]. Somatostatin acts also as a neuromodulator and neurotrans-mitter in the central nervous system and as a potent inhibitor of secretory processes. These actions as well as the reported antiproliferative effects of somatostatin [4-6] have stimulated the search for metabolically stabilized analoges for application in pharmacology and medicine [7]. Somatostatins exert their actions after binding to high affinity G protein-coupled receptors including five subtypes, $sst_{1-5}$ (sst= somatostatin subtype receptor). These receptors are expressed in a large variety of human tissues and are noticeably up-regulated in certain types of tumors, especially the $sst_2$ [10].

In a new promising approach, synthetic somatostatin analoges radiolabeled with a variety of metallic radionuclides have been used as alternative new routes to diagnosis and therapy of sst-expressing tumors [5,11-14]. These somatostatin derivatives are usually preserving the somatostatin pharmacophore core comprised by Phe-DTrp-Lys-Thr residues while carrying a suitable chelator at the N-terminus which serves as the metal binding site. Thus, the cyclic octapeptide octreotide (or Sandostatin) DPhe$^1$-Cys$^2$-Phe$^3$-DTrp$^4$-Lys$^5$-Thr$^6$-Cys$^7$-Thr$^8$-ol (disulfide bridged) [7,15-18] after coupling to suitable chelators, has been shown to effectively accommodate interesting diagnostic and/or therapeutic radionuclides, such as $^{111}$In [11], $^{99m}$Tc [20], $^{64}$Cu [21,22], $^{68}$Ga [23], $^{86}$Y [19] and others [22-26]. Recent data have shown that substitution of Phe$^3$ by Tyr$^3$ in the parent octreotide sequence as well as oxidation of the C-terminus alcohol to the corresponding carboxylic acid improves the accumulation of resulting radiopeptides at the tumor site by enhancing the affinity and selectivity of these agents for the

*Address correspondence to this author at the Department of Pharmacy, School of Health Sciences, University of Patras, Panepistimioupoli – Rion, GR-26504 Patras, Greece; Tel: ++30 2610 997 721; Fax: ++30 2610 997 713; E-mail: pacord@upatras.gr & G.A.Spyroulias@upatras.gr

Note: Atomic Coordinates of the energy minimized 20 best DYANA models and the mean energy minimized for (I) and (II) models have been deposited in the Protein Data Bank (accession codes 1y18 and 1y19, respectively).

1573-4064/05 $50.00+.00 

$sst_2$ as well as increasing their internalization capacity in $sst_2$-expressing cells [27,28,29].

We have been actively involved in the development of [$^{99m}$Tc]Demotate 1, a [Tyr$^3$]octreotate derivative functionalized with an open chain tetraamine donor atom set for enabling stable binding of $^{99m}$Tc. While unlabeled Demotate 1 exhibited high affinity binding to the $sst_2$ ($IC_{50}$= 0.13 nM), the radioligand, [$^{99m}$Tc]Demotate 1, displayed a favorable biodistribution profile in animal models [30]. Most importantly, [$^{99m}$Tc]Demotate 1 was capable to efficiently visualize $sst_2$-expressing lesions in a small number of carcinoid and pancreatic cancer patients [31,32].

In order to elucidate the factors operating in the high receptor affinity of Demotate 1, we report herein a comparative NMR study in DMSO of the following compounds: i) the parent peptide [Tyr$^3$]octreotate (DPhe$^1$-Cys$^2$-Tyr$^3$-DTrp$^4$-Lys$^5$-Thr$^6$-Cys$^7$-Thr$^8$-COOH; disulfide bridged), ii) Demotate 1 ($N_4$-DPhe$^1$-Cys$^2$-Tyr$^3$-DTrp$^4$-Lys$^5$-Thr$^6$-Cys$^7$-Thr$^8$-COOH; disulfide bridged) and iii) $N_4$-(Asp)$_2$-[Tyr$^3$]octreotate ($N_4$-Asp$^{-2}$-Asp$^{-1}$-DPhe$^1$-Cys$^2$-Tyr$^3$-DTrp$^4$-Lys$^5$-Thr$^6$-Cys$^7$-Thr$^8$-COOH; disulfide bridged), wherein a bis-negatively charged linker (Asp)$_2$ has been introduced between the $N_4$-moiety and the peptide backbone. Conformational features of these peptides are compared and discussed in the light of the NMR study of Sandostatin, attempting to evaluate the bioactive conformation of these somatostatin analogues.

## MATERIALS AND METHODS

### Peptide Synthesis and Purification

The [Tyr$^3$]octreotate was synthesized on the acid-sensitive 2-chlorotrityl chloride resin (substitution 0.6 mmol/g) [33] applying the Fmoc/tBu methodology [34]. The following side chain-protected amino acids were used: Fmoc-Cys (Mmt), Fmoc-Tyr(tBu), Fmoc-Thr(tBu), Fmoc-Lys(Boc), Fmoc-DTrp(Boc). The synthetic approach is illustrated at **Chart 1A** and details of the synthetic procedure have been published elsewhere [30]. The N,N',N'',N'''-tetra-(*tert*-butoxycarbonyl)-6-(carboxy)-1,4,8,11-tetraazaundecane ($N_4$

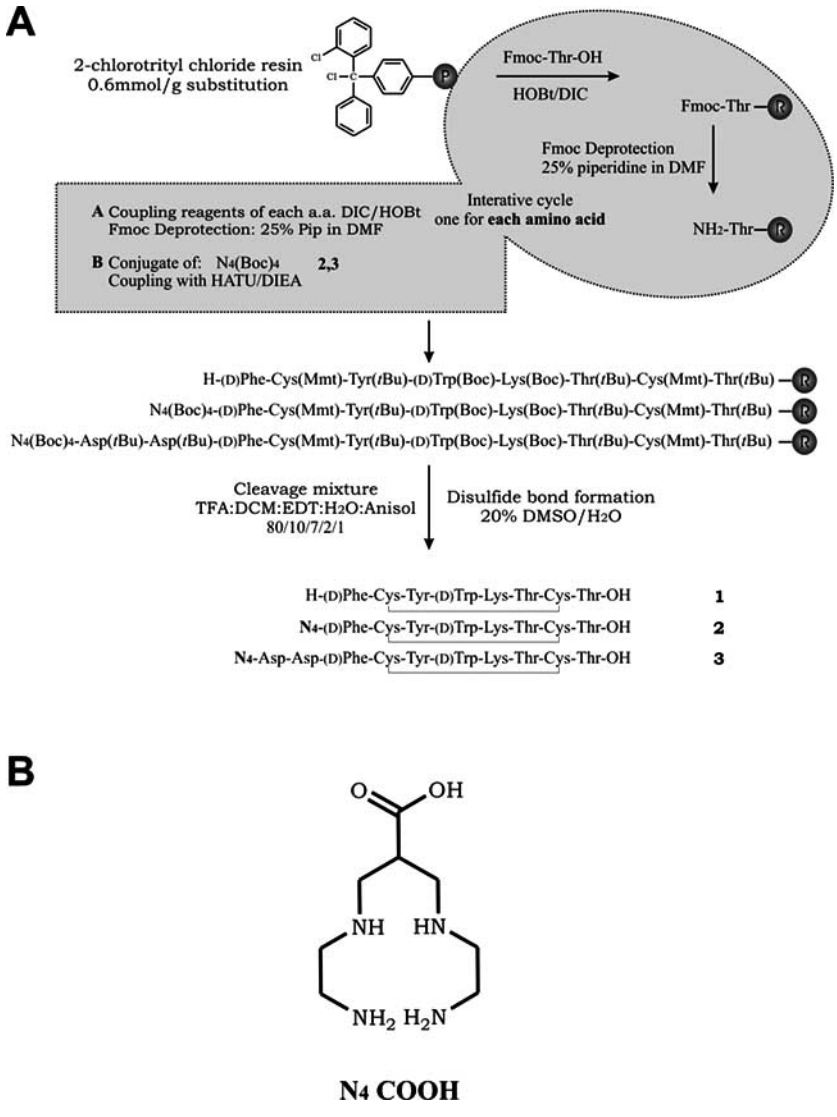


**Chart 1. (A)** Illustration of the strategy used for the synthesis of the peptides and the coupling of the tetraamine chelator, and **(B)** the molecular formula of the $N_4$ chelator.

chelator) was coupled to the terminal DPhe of the resin-immobilized peptide using a 3 molar excess of Boc-protected $N_4$, 3.3 molar excess of *O*-(7-azabenzotriazolyl-1,1,3,3-tetramethyluronium hexafluorophosphate (HATU) and 7 molar excess of diisopropylamine in DMF were reacted for 2 h. The chemical formula of the $N_4$ is illustrated at **Chart 1B**.

The peptides were cleaved from the resin after treatment with TFA: DCM (8:2) and the products were purified *via* Gel chromatography and RP-HPLC. After purification the synthesized peptides showed a purity of 95%. Dimethylsulfoxide DMSO-$d_6$ (MERCK) was used as deuterated solvent in NMR experiments and the peptides were dissolved to a final concentration of 2-2.5 mM in order to record 1D and 2D NMR spectra.

## NMR Spectroscopy

Data were acquired at 298K on a Bruker Avance 400-MHz spectrometer. $^1$H 1D NMR spectra were recorded using spectral width of 12-14 ppm with or without presaturation of the $H_2O$ signal. $^1$H-$^1$H 2D DQF-COSY [35], TOCSY [36] (Fig. **1**), were recorded using the MLEV-17 spin-lock sequence and $\tau_m$ = 80-100 ms. $^1$H-$^1$H TPPI NOESY [37,38] spectra (Fig. **1-2**) were acquired using $\tau_m$ 200-800 ms applying water suppression during the relaxation delay and mixing time [39]. All 2D spectra were acquired with 12 ppm spectral width, consisting of 2K data points in the F2 dimension, 16-32 transients and 1024 complex increments in the F1 dimension. Integration of NOESY cross-peak volumes was performed in maps acquired with $\tau_m \leq 400$ ms. Raw data were multiplied in both dimensions by a pure cosine-squared bell window function and Fourier-transformed to obtain 2048×2048 real data points. A polynomial base-line correction was applied in both directions. For data processing and spectral analysis, the standard Bruker software and XEASY program (ETH, Zürich) [40] were used.

## NOE Constraints

430, 462 and 493 NOESY ($\tau_m \leq 400$ ms) cross-peaks were assigned in both dimensions for [Tyr³]octreotate, $N_4$-[Tyr³]octreotate and $N_4$-$(Asp)_2$-[Tyr³]octreotate, respectively, in DMSO. The number of unique NOESY cross-peaks were 213, 229 and 258 (27, 23 and 24 constraints per residue for [Tyr³]octreotate, $N_4$-[Tyr³]octreotate and $N_4$-$(Asp)_2$-[Tyr³] octreotate, respectively, including the $N_4$ chelate group). Their intensities were converted into upper limit distances

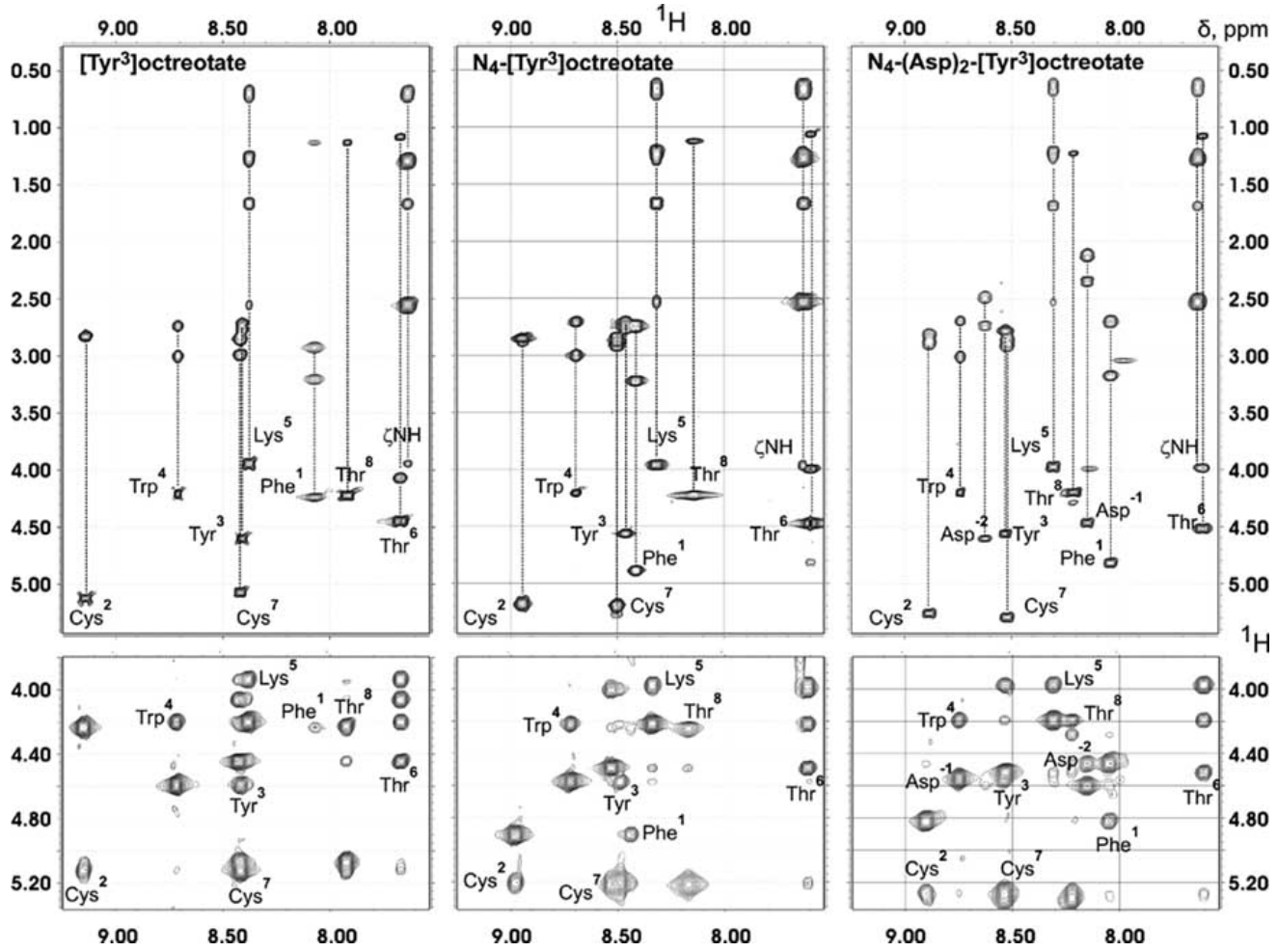


**Fig. (1).** Characteristic TOCSY (upper) and NOESY (lower) fingerprint regions of **(I), (II)** and **(III)** extracted from 2D $^1$H 400-MHz NMR recorded in DMSO-$d_6$ at 298 K. Hα-HN fingerprint region of NOESY spectra (lower panel) shows characteristic sequential connectivities.

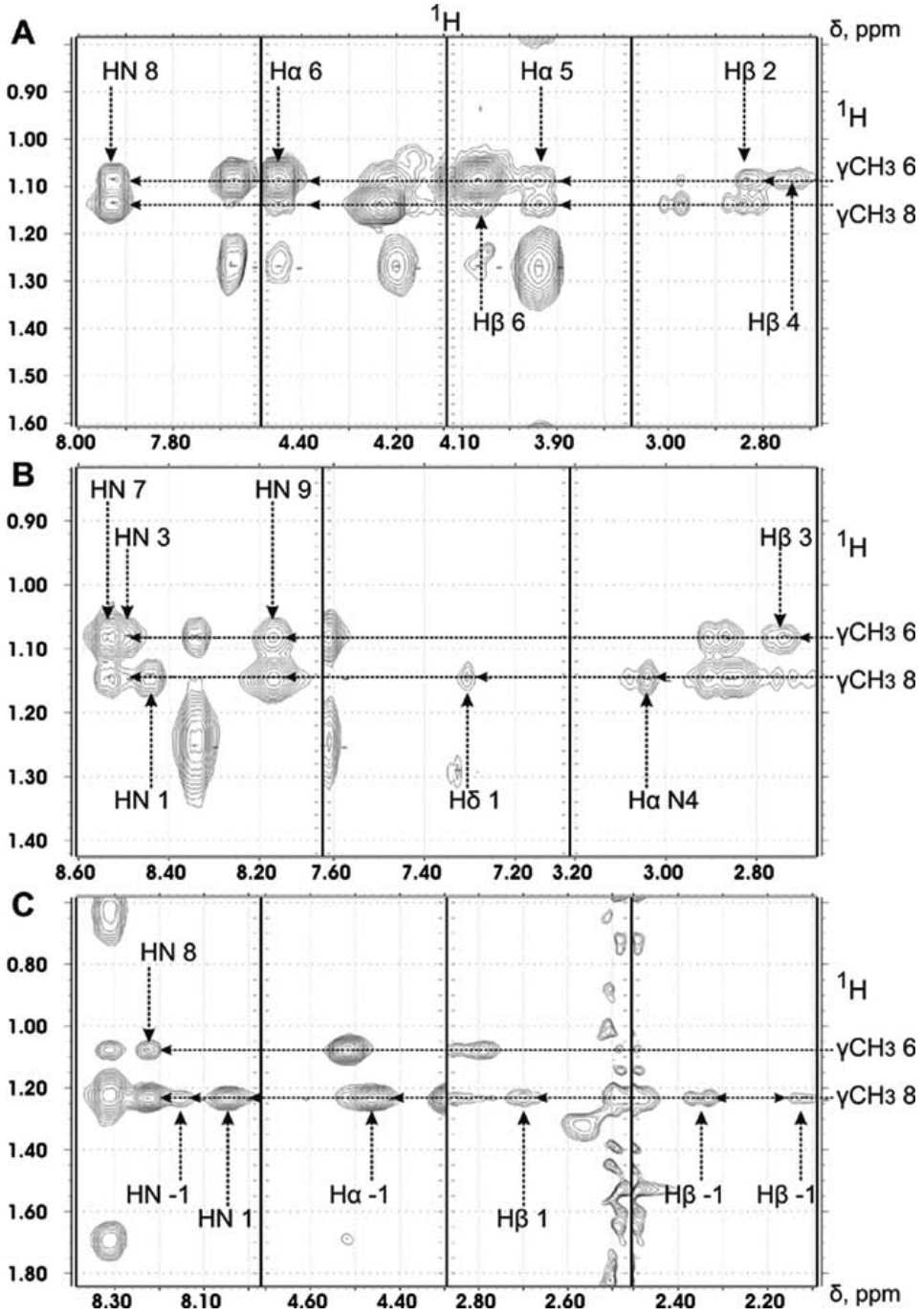


**Fig. (2).** Characteristic medium and long range NOESY cross peaks indicative between protons of Thr$^8$ and $N_4$, DPhe$^1$, Asp$^{-1}$ residues in [Tyr$^3$]octreotate **(A),** $N_4$-[Tyr$^3$]octreotate **(B),** and $N_4$-$(Asp)_2$-[Tyr$^3$]octreotate **(C)**.

through CALIBA [41]. Sequential constraints, number and range of NOEs are shown at Fig. **3,** while chemical shift differences ($\{(\Delta\delta_{H\alpha})^2 + (\Delta\delta_{HN})^2\}^{1/2}$) are illustrated in Fig. **4.**

### Structure Calculations and Refinement

Appropriate pseudoatom corrections were applied to methylene and methyl hydrogens. 154 NOE constraints for [Tyr$^3$]octreotate, 155 for $N_4$-[Tyr$^3$]octreotate and 199 for $N_4$-$(Asp)_2$-[Tyr$^3$]octreotate (19, 17 and 18 per residues, respectively, including the $N_4$ chelate group) were found meaningful and used in DYANA [42] calculations. The family ensemble of 20 best DYANA models (out of 400 calculated) in terms of target function and NOE violations (<0.2 Å), were refined through REM (AMBER 5.0 [43]; SANDER [44] program). A force constant of 133.76 kJ mol$^{-1}$ Å$^2$ is applied for the distance constraints. [Tyr$^3$]octreotate peptide models are illustrated in Fig. **5** (figures are generated with MOLMOL [45]). Structural calculations have been performed on IBM RISC6000 and xw4100 HP Linux workstations.

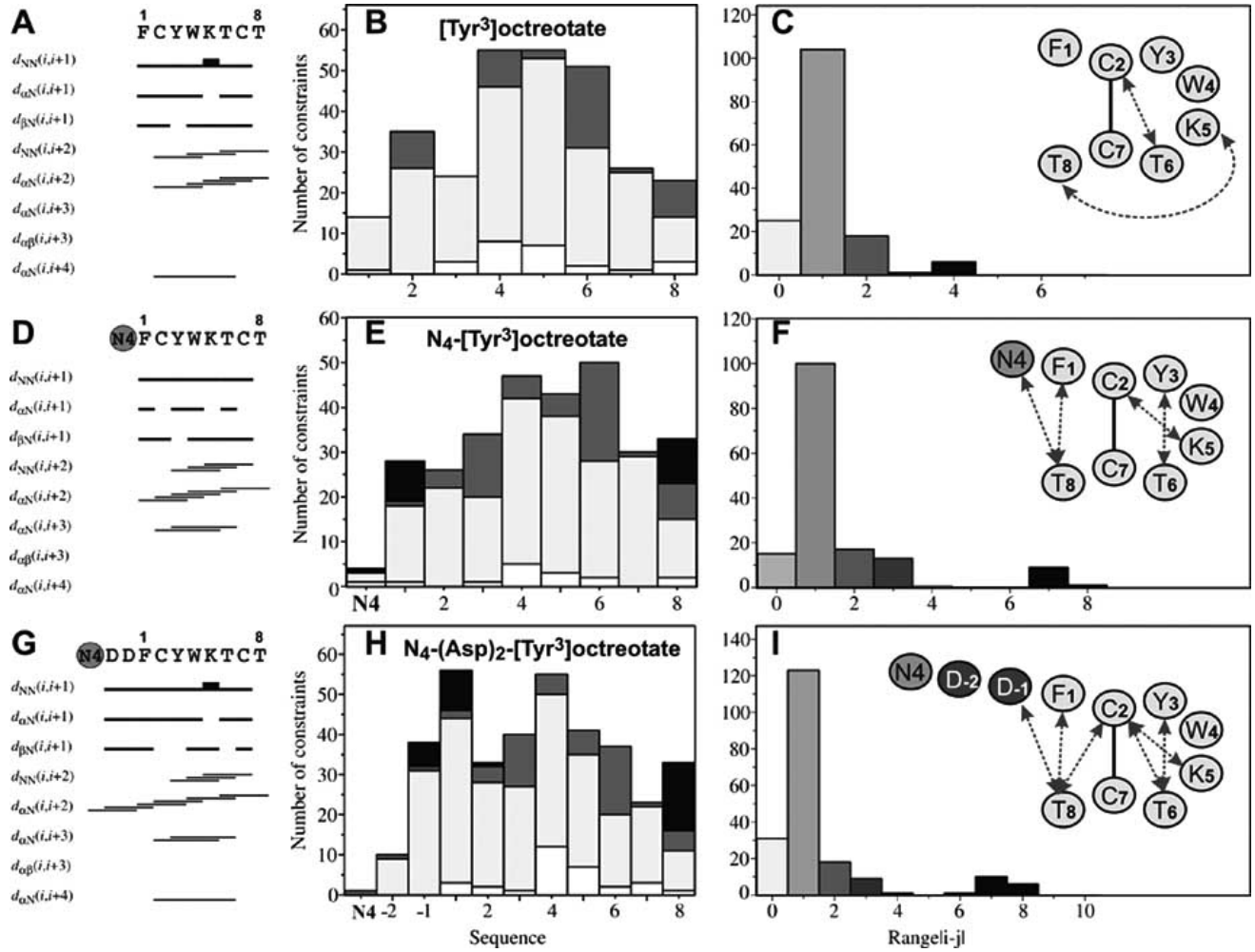


**Fig. (3).** Schematic representation of the sequential and medium-range NOE connectivities of **(I)**, **(II)** and **(III)** in DMSO (**A**, **D** and **G,** respectively). Number of NOE constraints per residue for each peptide for **(I)**, **(II)** and **(III)** is illustrated in **B**, **E** and **H**, respectively. White, gray, and dark gray vertical bars represent intraresidue, sequential and medium-range connectivities, respectively. NOE range for **(I)**, **(II)** and **(III)**, as well as characteristic long range NOE (indicated by arrows) are shown in **C**, **F** and **I,** respectively. All diagrams refer to meaningful NOE constraints extracted from $\tau_m$ = 400ms NOESY.

## RESULTS

### Proton Assignment

COSY and TOCSY maps were first analyzed to assign the individual spin patterns of amino acids through scalar connectivities. Sequential, medium and long range connectivities were identified from NOESY maps acquired with $\tau_m \geq$ 400 ms, and then assigned peaks transferred to maps acquired with $\tau_m \leq$ 400 ms. Integration of cross-peak intensities was performed in the latter spectra. Proton chemical shift peptides are reported in Table **1**.

### *[Tyr³]octreotate, (I)*

Numerous HN-HN, Hα-HN and Hβ-HN sequential connectivities are detected in the region Phe[1]-Cys[7], (see Fig. **3A**), while HN-HN and Hα-HN of (*i,i*+2) type connectivities are also identified between residues Cys[2]-DTrp[4], DTrp[4]-Thr[6] and Thr[6]-Thr[8]. An Hα-HN of (*i,i*+2) type connectivity between Lys[5]-Cys[7] has also been observed. Among the noteworthy NOEs are the long-range connectivities between the Cys[2] Hα – Thr[6] HN protons and that between the backbone (Hα) and side chain (Hγ) protons of Lys[5] and N-terminal residue Thr[8] (Fig. **3C**). The sequential NOE pattern is consistent with a $3_{10}$-helix turn comprised of the four (Lys-Thr-Cys-Thr) N-terminal residues of the sequence. An (*i,i*+3) hydrogen bond between the Thr[8] amide proton and the oxygen atom of Lys[5] has been observed in all 20 calculated models, further supporting the existence the C-terminal helix turn.

### *N₄-[Tyr³]octreotate, (II)*

The NOE pattern involving HN-HN, Hα-HN and Hβ-HN (*i,i*+1) connectivities for this peptide is rather similar to the non-functionalized peptide. HN-HN (*i,i*+2) type connectivities are observed only for the tripeptide comprised by Tyr[3]-Thr[6], while Hα-HN (*i,i*+2) type NOEs have been observed for

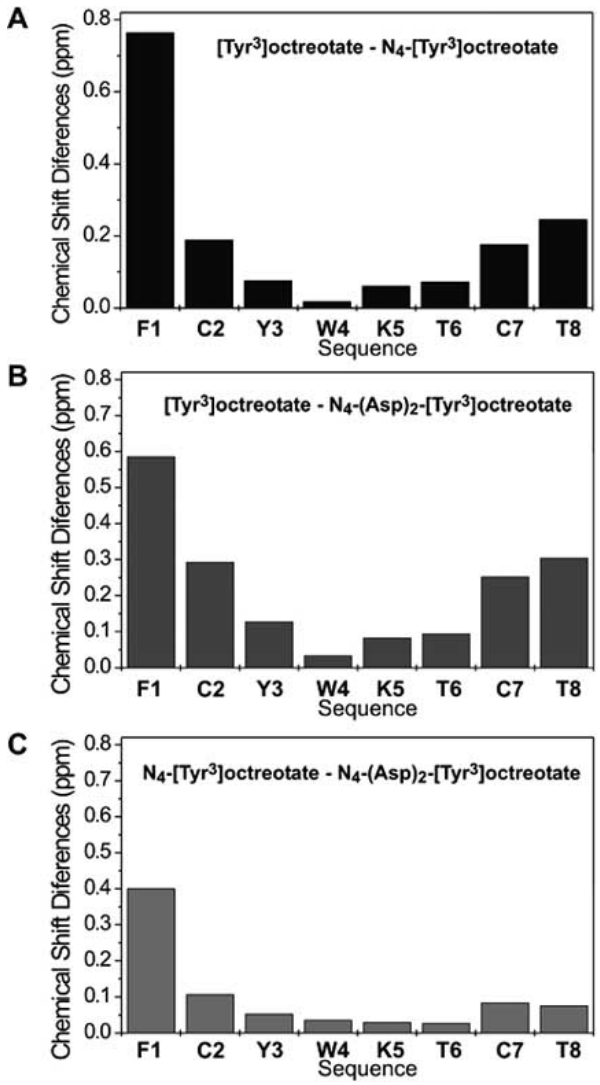


**Fig. (4).** Chemical shift variation (in ppm) plots between the $H^{-}$ and $H^{N}$ resonances of **(I)-(II) (A)**, **(I)-(III) (B),** and **(II)-(III) (C)**.

Phe[1]-Thr[6] fragment and for residues Thr[6]-Thr[8]. Hα-HN (*i,i*+3) NOEs between Cys[2]-Lys[5] and Tyr[3]-Thr[6] are also observed. The HN-HN and Hα-HN of Trp[4]-Thr[6] NOEs, in concert with Hα-HN between Tyr[3]-Thr[6], suggest a type I turn-like structure comprised of these residues. Additionally, nine long range NOEs of backbone and side-chain protons of Phe[1] and $N_4$ chelate group with Thr[8] indicate that the two termini of the peptide are in spatial proximity. No long-range connectivity between terminal residues has been observed in the non-functionalized peptide.

### *$N_4$-(Asp)$_2$-[Tyr$^3$]octreotate, (III)*

Hα-HN and HN-HN (*i,i*+2) type connectivities of this analog are rather similar to $N_4$ functionalized peptide while the Hα-HN (*i,i*+2) NOEs network involves the two N-terminal Asp residues. The two Hα-HN (*i,i*+3) NOEs observed in $N_4$-[Tyr[3]]octreotate between Cys[2]-Lys[5] and Tyr[3]-Thr[6] residues are still present in the $N_4$-(Asp)$_2$-[Tyr[3]]octreotate. Additionally an Hα-HN (*i,i*+4) NOE between Cys[2] and Thr[6], which was present in [Tyr[3]]octreotate but disappeared upon addition of the $N_4$-group, is now observed. Interestingly, a total number of 15 long-range NOEs between the N-terminal tripeptide segment of Asp-DPhe-Cys and the C-terminal Thr suggest that the two termini are in close proximity in a similar way as in $N_4$-[Tyr[3]]octreotate. This finding is also supported by the formation of a hydrogen bond between the amide proton of Thr[8] and the oxygen atom of the Phe[1] residue, for both peptides. However, in $N_4$-[Tyr[3]]octreotate no long-range NOE between the Cys[2] and the Thr[8] has been observed. Both $N_4$-[Tyr[3]]- and $N_4$-(Asp)$_2$-[Tyr[3]]- peptides form a turn comprised of Tyr[3]-DTrp[4]-Lys[5]-Thr[6] residues which, according to NOE pattern, bears the features of a type I turn structure.

Among the remarkable differences identified in NOESY spectra of the three peptides is the presence or the absence of characteristic NOE cross-peaks between protons belonging to C- and N- terminal residues. For example, in parent peptide **(I),** no NOE signal between Phe[1] and Thr[8] has been observed. In contrast, both **(II)** and **(III)** Phe[1]-Thr[8] exhibit long range NOE signals (8 and 9 NOEs, respectively), suggesting that the two termini of **(II)** and **(III)** peptides are in close spatial proximity. This is also supported by NOEs between the $N_4$ group (in **(II)**) and Asp residue (in **(III)**), and protons of C-terminal Thr[8]. More specifically, one NOE cross-peak was attributed to the interaction of the Hα proton of $N_4$ group with the $CH_3$ group of Thr[8], while five NOE cross-peaks were due to the interaction of the HN, Hα and Hβ Asp[-1] protons with Hβ (one connectivity) and $CH_3$ (four connectivities) protons of Thr[8]. Absence of NOE between $N_4$ group and C-terminal Thr[8] has been observed in **(III).** The absence of such NOEs is justified by the two intervening Asp residues, between the $N_4$ and Phe[1], shifting the $N_4$ chelate far from the C-terminal Thr[8]. On the other hand, Thr[8] in **(I)** gives rise to NOE contact through its $CH_3$ group to Hα proton of Lys[5]. The above data indicate different C-terminal conformation for the three peptides. Peptide **(I)** exhibits a helix turn at its 4-residue C-terminal fragment, while the same fragment seems to adopt a rather extended conformation in **(II)** and **(III)**.

Other meaningful differences in the NOE network were identified for the residues comprising the Cys[2]-Tyr[3]-DTrp[4]-Lys[5]-Thr[6]-Cys[7] ring. In **(I)**, Cys[2] Hα and Hβ protons are within NOE distance with Thr[6] HN, Hα and $CH_3$ giving rise to eight NOE cross peaks. On the other hand, no NOE was identified between Cys[2] and Lys[5]. However, two NOEs between Cys[2] Hα and Hβ protons and HN protons of Lys[5] were identified in **(II)**, while no NOE between Cys[2] and Thr[6] were observed for this peptide. In **(III)**, Cys[2] HN interacts with HN of Thr[8], while Cys[2] Hα interacts with HN of Lys[5] as well as with HN of Thr[6].

The NOE network involving the Tyr[3]-Trp[4]-Lys[5] residues of the three peptides, exhibits in all three peptides, NOE interactions between Cys[2] Hα/Hβ and DTrp[4] HN protons, while in **(I)** an additional Cys[2] HN – HN DTrp[4] NOE has been observed, as well. Tyr[3] HN proton gives rise to NOE signals with HN protons of DTrp[4] in all peptides, but in **(II)** and **(III)** Tyr[3] HN proton also gives rise to NOE signals with HN protons of Lys[5] and Thr[6]. NOEs involving the Tyr[3] Hα and the DTrp[4] HN, Hα, Hβ, Hδ1 protons (the latter

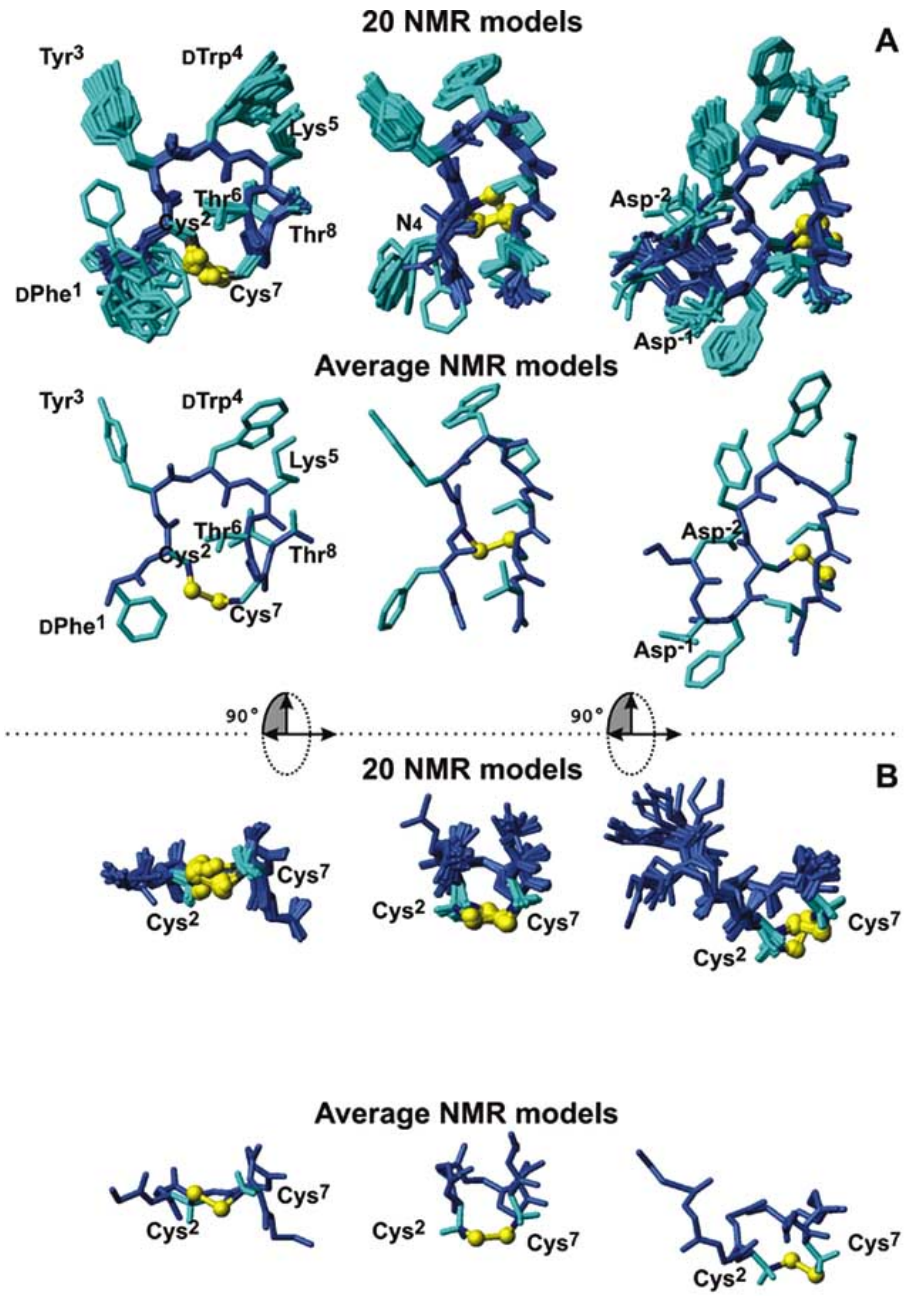


**Fig. (5). (A)** 20 REM models ensemble and mean REM structure of **(I), (II)** and **(III)**. **(B)** REM models rotated by 90º. Figure was generated with MOLMOL [45].

belonging to the pyrrole moiety of Trp indole ring) are common in all three peptides. However, there are considerable differences among the three peptides, with regard to the NOE network associated with $Tyr^3$ aryl ring and $DTrp^4$ protons. Specifically, in **(I)** only three weak NOEs have been observed between the Hδ and H of $Tyr^3$ ring and $DTrp^4$ backbone HN and Hα protons. In contrast, in **(II)** and **(III)** the Hδ and H protons of $Tyr^3$ ring are involved in six and nine NOE interactions, with HN and Hα protons of $DTrp^4$ (as in **(I)**), as well as with $DTrp^4$ Hβ protons and H 3 (with H $Tyr^3$) of aryl moiety of $DTrp^4$ indole ring. In **(I)** $DTrp^4$ pyrrole Hδ1 proton gives rise to NOE cross-peaks with practically all backbone and side chain protons (HN, Hα, Hβ, Hγ, Hδ and H ) of $Lys^5$. In **(II)** and **(III)**, $DTrp^4$ Hδ1 gives NOE signals with Hα, Hβ, Hγ and Hδ $Lys^5$ protons. Similarly, in **(I)** H 3 gives NOE signals with $Lys^5$ HN, Hα, Hγ and Hδ, while in **(II)** and **(III)** the only NOE signal observed between H 3 $DTrp^4$ and $Lys^5$ protons is that with HN proton. The variability observed for the side chain conformation of $Tyr^3$-$DTrp^4$-$Lys^5$ tripeptide fragment among the three peptides reflects the slightly different conformation of peptide backbone at this segment. Slight differences in the turn structure of the peptides have been also suggested by the analysis of the sequential NOE connectivities involving backbone protons.

**Table 1. Proton Chemical Shifts (ppm) of the Peptides at 298K (DMSO-$d_6$, 400 MHz)**

| Residue | | HN | Hα | Hβ | Other |
|---|---|---|---|---|---|
| **[Tyr$^3$]octreotate** | | | | | |
| 1 | DPhe | 8.074 | 4.234 | 3.195, 2.924 | Hδ 7.347 ; Hε 7.306 , Hζ 7.270 |
| 2 | Cys | 9.148 | 5.115 | 2.829 | ———————————— |
| 3 | Tyr | 8.417 | 4.592 | 2.769, 2.724 | Hδ 6.918 ; Hε 6.650 |
| 4 | DTrp | 8.718 | 4.201 | 3.001, 2.737 | Hε1 10.797, Hε3 7.441, Hζ2 7.332, Hδ1 7.067, Hη2 7.070, Hζ3 6.999 |
| 5 | Lys | 8.385 | 3.938 | 1.667 | Hγ 0.705, δCH$_3$ 1.267; εCH$_3$ 2.553 NHζ 7.641 |
| 6 | Thr | 7.674 | 4.445 | 4.064 | γCH$_3$ 1.085 |
| 7 | Cys | 8.422 | 5.071 | 2.969, 2.843 | ———————————— |
| 8 | Thr | 7.926 | 4.237 | 4.205 | γCH$_3$ 1.135 |
| **N$_4$-[Tyr$^3$]octreotate** | | | | | |
| - | N4 | | 3.042 | 2.663, 2.836 | Hδ 2.987, 3.036 ; Hε 2.852, 2.908 |
| 1 | DPhe | 8.441 | 4.903 | 3.241, 2.758 | Hδ 7.279 ; Hε 7.310 , Hζ 7.219 |
| 2 | Cys | 8.981 | 5.201 | 2.865, 2.908 | ———————————— |
| 3 | Tyr | 8.490 | 4.574 | 2.773, 2.740 | Hδ 6.930 ; Hε 6.660 |
| 4 | DTrp | 8.722 | 4.218 | 3.014, 2.728 | Hε1 10.800, Hε3 7.435, Hζ2 7.334, Hδ1 7.065, Hη2 7.067, Hζ3 7.008 |
| 5 | Lys | 8.341 | 3.979 | 1.686 | Hγ 0.672, δCH$_3$ 1.245; εCH$_3$ 2.545 NHζ 7.651 |
| 6 | Thr | 7.619 | 4.491 | 4.006 | γCH$_3$ 1.080 |
| 7 | Cys | 8.528 | 5.212 | 2.907, 2.872 | ———————————— |
| 8 | Thr | 8.171 | 4.246 | 4.276 | γCH$_3$ 1.144 |
| **N$_4$-(Asp)$_2$-[Tyr$^3$]octreotate** | | | | | |
| - | N4 | | 3.042 | 2.901 | 3.091, 2.932 |
| -2 | Asp | 8.628 | 4.598 | 2.741, 2.497 | ———————————— |
| -1 | Asp | 8.154 | 4.461 | 2.345, 2.117 | ———————————— |
| 1 | DPhe | 8.050 | 4.819 | 3.169, 2.702 | Hδ 7.278 ; Hε 7.236 , Hζ 7.181 |
| 2 | Cys | 8.899 | 5.268 | 2.889, 2.824 | |
| 3 | Tyr | 8.539 | 4.558 | 2.785 | Hδ 6.921 ; Hε 6.649 |
| 4 | DTrp | 8.751 | 4.198 | 3.014, 2.698 | Hε1 10.777, Hε3 7.418, Hζ2 7.331, Hδ1 7.048, Hη2 7.073, Hζ3 7.002 |
| 5 | Lys | 8.312 | 3.976 | 1.692 | Hγ 0.647, δCH$_3$ 1.276; εCH$_3$ 2.522 NHζ 7.634 |
| 6 | Thr | 7.614 | 4.517 | 3.982 | γCH$_3$ 1.081 |
| 7 | Cys | 8.540 | 5.294 | 2.882, 2.826 | |
| 8 | Thr | 8.227 | 4.196 | 4.287 | γCH$_3$ 1.233 |

## Chemical Shift Difference Analysis

Three diagrams illustrating the chemical shift differences between the peptides were plotted in order to illustrate the variation in chemical shifts imposed by the attachment of the $N_4$-chelator and the two Asp residues at the N-terminus. These plots refer to the peptide pairs **(I)-(II)** (see Fig. **4A**), **(I)-(III)** (see Fig. **4B**) and **(II)-(III)** (see Fig. **4C**). The largest chemical shift variations in all peptide pairs were

**Table 2. Statistical Analysis for the Final REM Structures of [Tyr³]Octreotate and Functionalized Derivatives**

| | [Tyr³]octreotate | | $N_4$-[Tyr³]octreotate | | $N_4$-$(Asp)_2$-[Tyr³]octreotate | |
|---|---|---|---|---|---|---|
| | REM [a] (20 models) | <REM> [a] | REM [a] (20 models) | <REM> [a] | REM [a] (20 models) | <REM> [a] |
| **RMS Violations per Experimental Distance Constraints (Å) [a]** | | | | | | |
| intraresidue (25/15/31) [b] | 0.0030 ± 0.0072 | 0.0000 | 0.0304 ± 0.0146 | 0.0254 | 0.0251 ± 0.0031 | 0.0259 |
| sequential (104/100/123) | 0.0160 ± 0.0033 | 0.0117 | 0.0145 ± 0.0050 | 0.0092 | 0.0145 ± 0.0032 | 0.0234 |
| medium-range (25/30/28) | 0.0231 ± 0.0047 | 0.0213 | 0.0305 ± 0.0055 | 0.0304 | 0.0167 ± 0.0116 | 0.0159 |
| long-range (0/10/17) | 0.0000 ± 0.0000 | 0.0000 | 0.0248 ± 0.0157 | 0.0183 | 0.0038 ± 0.0077 | 0.0000 |
| total (154/155/199) | 0.0166 ± 0.0025 | 0.0129 | 0.0220 ± 0.0043 | 0.0178 | 0.0172 ± 0.0020 | 0.0219 |
| **Average Number of Violations per Structure** | | | | | | |
| intraresidue | 0.1500 ± 0.3571 | 0.0000 | 1.4000 ± 0.6633 | 2.0000 | 1.0000 ± 0.0000 | 1.0000 |
| sequential | 4.7000 ± 1.3820 | 2.0000 | 3.1500 ± 1.1522 | 2.0000 | 3.6000 ± 1.2000 | 5.0000 |
| medium-range | 1.9000 ± 0.7681 | 2.0000 | 3.7000 ± 0.7141 | 4.0000 | 1.1500 ± 0.7921 | 2.0000 |
| long-range | 0.0000 ± 0.000 | 0.0000 | 0.9500 ± 0.5895 | 1.0000 | 0.2000 ± 0.4000 | 0.0000 |
| total | 6.7500 ± 1.479 | 5.0000 | 9.2000 ± 1.5684 | 9.0000 | 5.9500 ± 1.3592 | 8.0000 |
| average no. of NOE violations > than 0.3 Å | 0.000 | 0.000 | 0.000 | 0.000 | 0.000 | 0.000 |
| largest residual NOE violation (Å) | 0.172 | 0.085 | 0.239 | 0.112 | 0.170 | 0.158 |
| average distance penalty function ($Å^2$) | 1.627 ± 0.400 | 1.102 | 2.937 ± 1.000 | 2.109 | 2.558 ± 0.400 | 3.480 |

[a] REM indicates the energy-minimized ensemble of 20 models and <REM> the mean energy-minimized model.

[b] Numbers in parenthesis indicate the number of meaningful upper distance limits per class.

observed for Phe[1] and Cys[2], while noticeable chemical shift differences are calculated for the two last residues of the peptide sequences, in **(I)-(II)** and **(I)-(III)**. For these pairs the smallest chemical shift difference is calculated first for DTrp[4] and then for Lys[5], which are sited at the middle of the sequence. The **(I)-(II)** and **(I)-(III)** chemical shift difference plots are quite similar, with the main difference being the smaller variation (> 0.75 ppm for **(I)-(II)** and < 0.6 ppm for **(I)-(III)**) for the proton resonances of Phe[1]. This is apparently due to the fact that the $N_4$ chelate bearing two mobile branches in **(II)** has been attached next to Phe[1] while in the case of **(III)** this group has been shifted two positions away by the insertion of two additional Asp residues. The greater impact of the $N_4$-group on chemical shifts of Phe[1] among the three peptides is illustrated by the **(II)-(III)** plot (see Fig. **4C**). The insertion of the Asp residues quantified by the $(\{(\Delta\delta_{H\alpha})^2 + (\Delta\delta_{HN})^2\}^{1/2})$ difference for Phe[1] is half (0.4 ppm for **(II)-(III)**; see Fig. **4C**) to that observed when the $N_4$-group is directly attached to Phe[1] (> 0.75 ppm for **(I)-(II)**; see Fig. **4A**). Additionally, noticeable chemical shift differences close to or larger than 0.2 ppm have been observed in **(I)-(II)** and **(I)-(III)** for Cys[7] and Thr[8]. However, these differences are considerably small in the **(II)-(III)** pair, suggesting larger conformational rearrangements between [Tyr³]octreotate and **(II)**/**(III)** peptides than between the two [Tyr³]octreotate derivatives **(II)** and **(III)**.

### Structure Calculations and Conformational Analysis

The NOE-derived structural information extracted from the analysis of NOESY spectra acquired in DMSO solutions under identical experimental condition for mixing time $\tau_m$ = 400 msec was introduced to DYANA software for structure calculation. The average target function for the DYANA family of 20 calculated models (Fig. **5A**) was found to be $0.14 \pm 1.57 \times 10^{-2}$ $Å^2$ for **(I)**, $0.32 \pm 0.15$ $Å^2$ for **(II)** and $0.15 \pm 2.42 \times 10^{-2}$ $Å^2$ for **(III)** models (**Fig 5B**). The final **(I)** REM models exhibit pairwise rmsd values for all residues 0.33 ± 0.14 Å (BB), 1.33 ± 0.42 Å (HA) for the 20 structures and 0.23 ± 0.09 Å (BB), 0.91 ± 0.31 Å (HA) for the mean structure (Fig. **5A**), respectively. The rmsd values for **(II)** (all residues except $N_4$ chelate group) REM ensemble are 0.31 ± 0.11 Å (BB), 0.90 ± 0.26 Å (HA) for the 20 models and 0.21 ± 0.07 Å (BB), 0.62 ± 0.18 Å (HA) for the mean structure (Fig. **5B**) while for **(III)** (residues Phe[1] to Thr[8]) they are 0.35 ± 0.21 Å (BB), 0.80 ± 0.23 Å (HA) for the 20 models and 0.27 ± 0.08 Å (BB), 0.59 ± 0.11 Å (HA) for the mean structure, respectively. Statistical data for REM models and average structure are given in Table **2**.

## DISCUSSION

According to the NMR analysis (Fig. **3 & 4**) and structure calculations (Fig. **5**) presented here, [Tyr$^3$]octreotate **(I)** differs from both $N_4$-[Tyr$^3$]octreotate **(II)** and $N_4$-(Asp)$_2$-[Tyr$^3$]octreotate **(III)** while the latter two peptides share some similar conformational features. Indeed, only in **(II)** and **(III)** the N- and C- residues are found in close proximity as manifested by long range NOEs. These NOEs between Asp$^{-1}$/DPhe$^1$ and Thr$^8$ indicate that these molecules adopt a $\beta$-sheet antiparallel fold with a more constrained Tyr$^3$-Thr$^6$ loop than in the case of unmodified [Tyr$^3$]octreotate.

The main difference in skeleton of the three peptides is located on their C-terminal structure. Only in the case of [Tyr$^3$]octreotate peptide, residues Thr$^6$, Cys$^7$ and Thr$^8$ form a turn-like structure partially resembling a $3_{10}$ helix conformation (see Fig. **3A-C**), which is supported by NOEs between Lys$^5$ with Thr$^8$. The only difference between peptides **(I)** and **(II)** is the presence of the $N_4$-chelator. However, **(I)** exhibits a turn like structure while **(II)** exhibits an extended conformation. Attachment of this $N_4$ group is not expected to influence the C-terminal residues directly, but the N-terminal DPhe$^1$ and Cys$^2$ residues. Indeed, what is observed is a variation in Cys$^2$ – Cys$^7$ disulfide bridge geometry. In [Tyr$^3$] octreotate the disulfide bridge lies in the plane of the Cys$^2$-Cys$^7$ skeleton atoms, while in the other two peptides this seems to decline. In the latter case, residues Thr$^6$-Cys$^7$-Thr$^8$ adopt an extended structure. Therefore, chemical modifications and/or addition of a new group at the N-terminus may influence the conformational flexibility of Cys$^2$, which in turn affects the geometry of Cys$^2$-Cys$^7$ disulfide bridge and finally the conformation of side- and main-chain of Cys$^7$ sited at the C-terminus.

The orientation of the side chains of DTrp$^4$ and Lys$^5$, which are sited in the $\beta$-turn region, differs in the three analogs. In [Tyr$^3$]octreotate, the DTrp$^4$ indole ring is in close proximity to the Lys$^5$ side-chain rather than the Tyr$^3$ residue. In **(II),** the DTrp$^4$ indole moiety changes its orientation, and orients towards Tyr$^3$ aryl ring. In **(III)**, the DTrp$^4$ indole conformation, is closer to that found for **(II)** than that found for **(I)**. Additionally, the DPhe$^1$ side chain in [Tyr$^3$]octreotate, is orientated toward the disulfide bridge, in contrast to $N_4$-[Tyr$^3$]octreotate and $N_4$-(Asp)$_2$-[Tyr$^3$] octreotate, where the aromatic rings of DPhe$^1$ and Tyr$^3$ are oriented towards the same direction, approaching each other. Especially in the case of $N_4$-[Tyr$^3$]octreotate, new NOE signals between the aromatic rings of Phe$^1$ and Tyr$^3$ are observed.

The [Tyr$^3$]octreotate octapeptide presented in this paper closely resembles Sandostatin (octreotide), which has been the subject of extensive conformational studies in solid state [46] and in solution [16,47-49]. Until 1997, [46-49] solution NMR studies in a variety of solvents, such as water, DMSO, water/MeOH mixture etc., have revealed that Sandostatin adopts a predominant antiparallel $\beta$-sheet conformation characterized by a type II' $\beta$-turn spanning DTrp$^4$-Lys$^5$ residues. In 1995, an X-ray study of Sandostatin revealed that the octapeptide co-crystallizes in three different conformations [46]. The asymmetric unit of Sandostatin crystals contained one molecule with conformational characteristics rather similar to those revealed by the above mentioned NMR solution studies. However, the asymmetric unit also contained two Sandostatin molecules, which with respect to the former bear a similar structure for the residues DPhe$^1$-Lys$^5$, but different conformation for the C-terminal tripeptide. This fragment spanning residues Thr$^6$-Cys$^7$-Thr$^8$ seems to fold into a helical turn stabilized by two hydrogen bonds, formed by Cys$^7$ NH – DTrp$^4$ C=O and Phe$^3$ NH – Thr$^6$ OH residues. In 1997, a detailed NMR analysis of Sandostatin by Goodman *et al*. revealed an equilibrium between the $\beta$-sheet and partially helical conformations. They reported that NOE data extracted from the NMR spectra acquired in DMSO-$d_6$ solution are not consistent either with the $\beta$-sheet model or with the partially helical conformation. Instead, some of these NOEs are consistent with the former and others with the latter conformation.

[Tyr$^3$]octreotate differs from Sandostatin at two sites: (i) position 3 of the sequence, where a Tyr residue replaces Phe and (ii) the C-terminus, where [Tyr$^3$]octreotate bears a carboxy terminal group in contrast to the alcoholic C-terminal group of Sandostatin. This peptide, **(I),** studied under the experimental conditions described above in solution (DMSO-$d_6$, 298K) through NMR, seems to adopt a unique 3D-structure characterized by the cyclic, disulfide bridged, peptide core, comprised of the residues Cys$^2$-Tyr$^3$-DTrp$^4$-Lys$^5$-Thr$^6$-Cys$^7$, while the C-terminus is characterized by a turn structure including Thr$^6$-Cys$^7$-Thr$^8$ residues. None long range NOE between the N-/C- terminal residues has been identified as illustrated in Fig. **3B & C,** declining the presence of a fraction of an antiparallel $\beta$-sheet conformation. Therefore, in the present study the calculated NMR [Tyr$^3$]octreotate models converge toward only one conformation state; that is the partially helical conformation. As mentioned above, these data are further supported by the sequential NOE pattern for the C-terminal tripeptide fragment and the NOE between the Thr$^8$ $\gamma CH_3$ and the Lys$^5$ H$\alpha$ protons.

Best fit of the backbone atoms of the [Tyr$^3$]octreotate NMR average minimized structure and Sandostatin, partially helical, NMR conformers available in Protein Data Bank (pdb code: 2soc) reveals great structural similarities (see Fig. **6A**). The two models differ slightly to the disulfide bridge geometry. In Sandostatin, the disulfide bridge, declines from the plane defined by the Cys$^2$-Cys$^7$ backbone atoms that seem to lie at the same plane. In contrast the Cys$^2$-Cys$^7$ disulfide bridge in [Tyr$^3$]octreotate seem to flip out of the plane defined by the backbone atoms of Cys$^2$-Lys$^5$ and Cys$^7$ residues and lies on the plane of the Cys$^2$-Thr$^6$ backbone atoms.

In contrast, significant differences are observed when best fit among the [Tyr$^3$]octreotate and Sandostatin, antiparallel $\beta$-sheet, NMR conformer [pdb code: 1soc], is attempted. Apart from the remarkable difference in the C-terminal tripeptide structure, differences in conformation of the Tyr/Phe$^3$-DTrp$^4$-Lys$^5$ backbone are also observed. The Tyr/Phe$^3$-Thr$^6$ C$\alpha$-C$\alpha$ interatomic distance is 7.0 Å in [Tyr$^3$]octreotate, while the same distance in sandostatin model measured 5.3 Å (6.0 in "$\alpha$-helix" model; see Fig. **6A**). These data suggest that the attachment of the $N_4$-group to [Tyr$^3$]octreotate peptide imposes a $\beta$-sheet antiparallel structure, which also affects the loop formed by the fragment

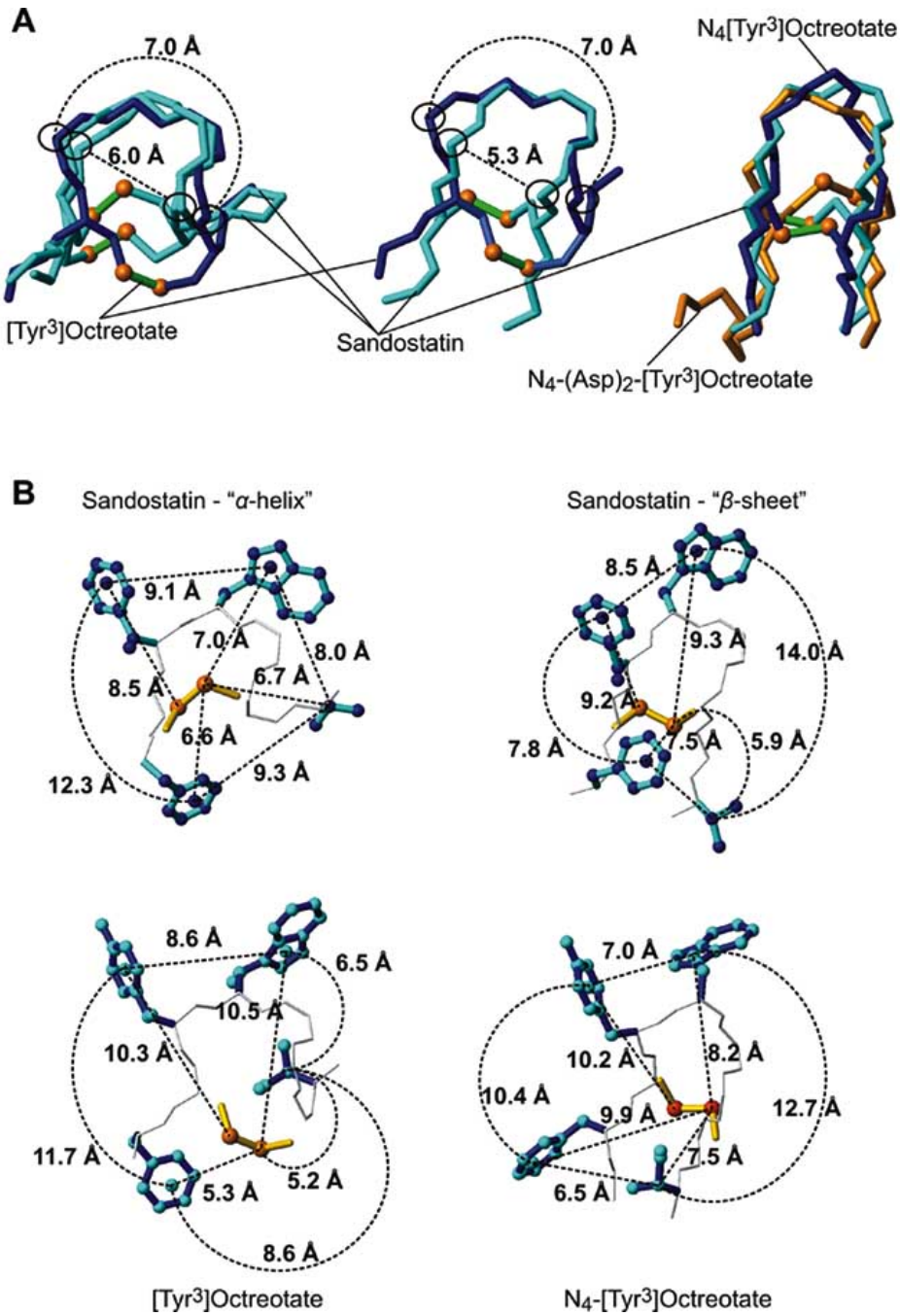


**Fig. (6). (A)** Best fit of mean, energy minimized, models of [Tyr³]octreotate (blue) and Sandostatin "α-helix" two models (cyan), [Tyr³]octreotate (blue) and Sandostatin "β-sheet" models (cyan), and **(C)** $N_4$-[Tyr³]octreotate (blue), $N_4$-$(Asp)_2$-[Tyr³]octreoate (orange red) and Sandostatin (cyan). **(B)** Distances between key residues in Sandostatin (upper) and [Tyr³]octreotate models (lower).

of $Tyr^3$-$Thr^6$ residues. In this case, the turn is formed by $Tyr^3$-$DTrp^4$-$Lys^5$, while in [$Tyr^3$]octreotate α-helical structure a less constrained loop is formed by the four residues $Tyr^3$-$DTrp^4$-$Lys^5$-$Thr^6$. However, the distance between the Cβ atoms of $Cys^2$ and $Cys^7$ is found to remain practically the same (4.1 and 4.2 Å in [$Tyr^3$]octreotate and Sandostatin models, respectively). Finally, the two terminal residues $DPhe^1$ and the $Thr^8$ are found in close spatial proximity only in the Sandostatin model, at a distance of 6.0 Å (measured in Cα atoms) while the same distance is 10.3 Å in [$Tyr^3$]octreotate. For detailed analysis of distances between key residues of Sandostatin models and [$Tyr^3$]octreotate peptides **(I)** and **(II),** see Fig. **6B.**

Overall, the [$Tyr^3$]octreotate peptide exhibits a similar fold with the "α-helical" model of Goodman *et al*. [16], while $N_4$-[$Tyr^3$]octreotate resembles the "β-sheet" model, originally proposed in the mid-80's, and also determined through NMR by Goodman *et al*. [16]. According to our NMR studies, attachment of the tetraamine chelator or extension of the N-terminal peptide sequence by two Asp

residues in [Tyr$^3$]octreotate impose some structural rearrangements to the peptide which led to an extended conformation of the C-terminal conformation. These rearrangements are focused on the variation of: (i) the geometry of the disulfide bridge, (ii) the aromatic residues DPhe$^1$/Tyr$^3$ and the $\beta$-turn residues DTrp$^4$-Lys$^5$ side chain orientation, and (iii) the conformation of the C-terminal tripeptide. According to mounting evidence in the literature, some of these residues are thought to play an important role in somatostatin-like activity of these peptides [17,30-32].

## CONCLUDING REMARKS – BIOLOGICAL IMPLICATIONS

Somatostatin analogs, such as [Tyr$^3$]octreotate and Sandostatin, are known to elicit somatostatin-like bioactivity [15]. The somatostatin pharmacophore model is associated with the conformational features of DTrp$^4$ and Lys$^5$ residues, the geometry of the disulfide bridge and the aromatic residues at a distance of approximately 9 Å from both DTrp$^4$ and Lys$^5$. Such kind of conformational features are found in the case of Sandostatin in the "$\beta$-sheet" model [16], and are fully consistent with previous data that have indicated the $\beta$-sheet structure as the somatostatin-like bioactive conformation.

Coupling of an open chain tetraamine chelator directly at the N-terminus of [Tyr$^3$]octreotate (Demotate 1) enables facile labeling with the diagnostic radionuclide $^{99m}$Tc under formation of a stable and polar monocationic $^{99m}$Tc-chelate. Both unlabeled and labeled peptide [$^{99m}$Tc-N$_4$,Tyr$^3$]octreotate ([$^{99m}$Tc]Demotate 1) showed high affinity binding in sst$_2$-expressing tissues and sst$_2$-positive cells. It is interesting to note that the affinity of the unlabeled peptide (Demotate 1) for the sst$_2$ was found to be high (IC$_{50}$= 0.13 nM) exceeding that of unmodified parent peptides [Tyr$^3$]octreotate (IC$_{50}$= 0.30 nM) or [Tyr$^3$]octreotide (IC$_{50}$= 0.46 nM) (Phe$^3$→Tyr$^3$ Sandostatin) [30]. [$^{99m}$Tc]Demotate 1 showed excellent *in vivo* properties in tumor-bearing rodents that translated into excellent tumor images in neuroendocrine tumor patients in a Pilot/Phase I clinical study. The introduction of negatively charged Asp linker(s) between the radiometal-chelate and the [Tyr$^3$]octreotate moiety has been shown to affect these properties [50,51]. In particular, addition of two Asp residues was found to cause a drop in the affinity versus the sst$_2$ by more than a power of ten (IC$_{50}$= 2.30 nM). Furthermore, internalization of the radiolabeled peptide in sst$_2$-expressing cells and uptake in sst$_2$-positive organs and experimental tumors in rodents were found much inferior in comparison to [$^{99m}$Tc]Demotate 1 [50,51]. These findings prompted us to investigate conformational differences between analogs **(II)** and **(III)** and relate them to the parent unmodified peptide **(I)**.

According to structural analysis of [Tyr$^3$]octreotate and its analogs, the N$_4$-functionalized [Tyr$^3$]octreotate derivative **(II)** exhibits $\beta$-sheet structure. The Lys$^5$ NH$_3$ group is within a distance of 7.0 to 7.8 Å from Cys$^7$ and Cys$^2$ sulfur atoms, while Hδ1 atom of DTrp$^4$ indole group is at a distance of 8.0 Å from sulfur atoms of both Cys residues. The IC$_{50}$ value of 0.13 nM determined for **(II)** suggests that the presence of the N$_4$-group at the immediate vicinity of the peptide enhances binding affinity. In contrast, extension of the peptide chain by two negatively-charged Asp residues significantly impairs binding affinity by more than one order of magnitude (IC$_{50}$= 2.30 nM). Although the extension of peptide chain does not considerably alter the general feature of the peptide's pharmacophore model ($\beta$-sheet conformation, disulfide bridge geometry, DTrp$^4$-Lys$^5$ orientation, etc.), the introduction of two more residues seems to have greatly altered receptor affinity. These two N-terminal Asp residues provide a net charge of -2, while forming a flexible turn-like tail. Considering that $\beta$-sheet model of Sandostatin is the bioactive conformation and that [Tyr$^3$]octreotate, which exhibits a C-terminal helix, is less active than the N$_4$-[Tyr$^3$]octreotate, it might be concluded that presence of a helix turn might diminish the binding affinity of these peptides for the sst$_2$. It is well established, that binding involves both electrostatic interactions and shape complementarity, and these factors apparently differ between N$_4$-[Tyr$^3$]octreotate and N$_4$-(Asp)$_2$-[Tyr$^3$]octreotate suggesting that $\beta$-sheet conformation should be a prerequisite in the design of new bioactive somatostatin analogs.

## ACKNOWLEDGEMENTS

The General Secretariat of Research and Technology and Ministry of Education of Greece - "Pythagoras" Program and the U of Patras, for a K. Karatheodoris Research Grant, are acknowledged for their financial support.

## ABBREVIATIONS

| | | |
|---|---|---|
| N$_4$ | = | Tetraamine chelator |
| DQF-COSY | = | Double-Quantum-Filtered phase sensitive Correlated SpectroscopY |
| NOE | = | Nuclear Overhauser Effect |
| TOCSY | = | Total Correlation SpectroscopY |
| NOESY | = | Nuclear Overhauser Effect SpectroscopY |
| DYANA | = | DYnamic Algorithm for Nmr Applications |
| RMSD | = | Root Mean-Square Deviation |
| REM | = | Restrained Energy Minimization |

## REFERENCES

[1] Weckbecker, G.; Lewis, I.; Albert, R.; Schmid, H.A.; Hoyer, D.; Bruns, C. *Nat. Rev. Drug Discov*., **2003,** *2,* 999.
[2] Reichlin, S. *N. Engl. J. Med*., **1983,** *309,* 1495.
[3] Reichlin, S. *N. Engl. J. Med.,* **1983,** *309,* 1556.
[4] Yamada, Y.; Post, S.R.; Wang, K.; Tager, H.S.; Bell, G.I.; Seino, S. *Proc. Natl Acad. Sci. USA*, **1992,** *89,* 251.
[5] Weckbecker, G.; Raulf, F.; Stolz, B.; Bruns, C. *Pharmac. Ther*., **1993,** *60,* 245.
[6] Gillies, G. *Trends Pharmacol. Sci*., **1997,** *18*, 87.
[7] Kaupmann, K.; Bruns, C.; Raulf, F.; Weber, H.P.; Mattes, H.; Lubbert, H. *EMBO J*, **1995,** *14,* 727.
[8] Reubi, J.C.; Perrin, M.H.; Rivier, J.E.; Vale, W. *Life Sci*., **1981,** *28,* 2191.
[9] Ensinck, J.W.; Baskin, D.G.; Vahl, T.P.; Vogel, R.E.; Laschansky, E.C.; Francis, B.H.; Hoffman, R.C.; Krakover, J.D.; Stamm, M.R.; Low, M.J.; Rubinstein, M.; Otero-Corchon, V.; D'Alessio, D.A. *Endocrinology*, **2002,** *143*, 2599.
[10] Reubi, J.C.; Kvols, L.K.; Krenning, E.P.; Lamberts, S.W.J. *Metabolism*, **1990**, *39,* 78.

[11] Bakker, W.H.; Albert, R.; Bruns, C.; Breeman, W.A.P.; Hofland, L.J.; Marbach, P.; Pless, J.; Pralet, D.; Stolz, B.; Koper, J.W.; Lamberts, S.W.J.; Visser, T.J.; Krenning, E.P. *Life Sci*., **1991,** *49,* 1583.

[12] Stolz, B.; Weckbecker, G.; Smith-Jones, P.M.; Albert, R.; Raulf, F.; Bruns, C. *Eur. J. Nucl. Med*., **1998,** *25,* 668.

[13] Virgolini, I.; Traub, T.; Novotny, C.; Leimer, M.; Fuger, B.; Li, S.R.; Patri. P.; Pangerl, T.; Angelberger, P.; Raderer, M.; Burggasser, G.; Andreae, F.; Kurtaran, A.; Dudczak, R. *Curr. Pharm. Des.*, **2002,** *8,* 1781.

[14] De Jong, M.; Valkema, R.; Jamar, F.; Kvols, L.K.; Kwekkeboom, D.J.; Breeman, W.A.; Bakker, W.H.; Smith, C.; Pauwels, S.; Krenning, E.P. *Sem. Nucl. Med*., **2002,** *32,* 133.

[15] Bauer, W.; Briner, U.; Doepfener, W.; Haller, R.; Huguenin, R.; Marbach, P.; Petcher, T.J.; Pless, J. *Life Sci*., **1982**, *31*, 1133.

[16] Melacini, G.; Zhu, Q.; Goodman, M. *Biochemistry*, **1997,** *36,* 1233.

[17] Rueter, J.K.; Mattern, R.H.; Zhang, L.; Taylor, J.; Morgan, B.; Hoyer, D.; Goodman, M. *Biopolymers*, **2000**, *53,* 497.

[18] Mattern, R.H.; Zhang, L.; Rueter, J.K.; Goodman, M. *Biopolymers*, **2000,** *53,* 506.

[19] Wester, H.J.; Brockmann, J.; Rösch, F.; Wutz, W.; Herzog, H.; Smith-Jones, P.; Stolz, B.; Bruns, C.; Stöcklin, G. *Nucl. Med. Biol*., **1997,** *24,* 275.

[20] Maina, T.; Stolz, B.; Albert, R.; Bruns, C.; Koch, P.; Mäcke, H. *Eur. J. Nucl. Med*., **1994,** *21,* 437.

[21] Anderson, C.J.; Pajeau, T.S.; Edwards, W.B.; Sherman, E.L.C.; Rogers, B.E.; Welch, M.J. *J. Nucl. Med*., **1995,** *36,* 2315.

[22] Lewis, J.S.; Srinivasan, A.; Schmidt, M.A.; Anderson, C.J. *Nucl. Med. Biol*., **1999,** *26,* 267.

[23] Smith-Jones, P.M.; Stolz, B.; Bruns, C.; Albert, R.; Reist, H.W.; Friedrich, R.; Mäcke H.R. *J. Nucl. Med*., **1994,** *35,* 317.

[24] Bakker, W.H.; Krenning, E.P.; Breeman, W.A.; Kooji, P.P.M.; Reubi, J.C.; Koper, J.W.; De Jong, M.; Lameris, J.S.; Visser, T.J., Lamberts S.W.J. *J. Nucl. Med.*, **1991,** *32,* 1184.

[25] Breeman, W. A.P.; Hofland, L.J.; Bakker, W.H.; van der Pluijm, M.; van Koetsveld, P.M.; De Jong, M.; Setyono-Han, B.; Kwekkeboom, D.J.; Visser, T.J.; Lamberts, S.W.J.; Krenning E.P. *Eur. J. Nucl. Med*., **1993,** *20,* 1089.

[26] Lamberts, S.W.J.; Bakker, W.H.; Reubi, J.C.; Krenning E.P. *J. Steroid Biochem. Mol. Biol*., **1990,** *37,* 1079.

[27] De Jong, M.; Bakker, W.H.; Breeman, W.A.P.; Bernard, W.H.; Hofland, L.J.; Visser T.J.; Srinivasan, A.; Schmidt, M.; Béhé, M.; Mäcke, H.R.; Krenning E.P. *Int. J. Cancer*, **1998,** *75,* 406.

[28] De Jong, M.; Breeman, W.A.P.; Bakker, W.H.; Kooji, P.P.M.; Bernard, B.F.; Hofland, L.J.; Visser, T.J.; Srinivasan, A.; Schmidt, M.A.; Erion, J.L.; Bugai, J.E.; Mäcke, H.R.; Krenning, E.P. *Cancer Res*., **1998,** *58,* 437.

[29] Reubi, J.C.; Schär, J.-C.; Waser, B.; Wenger, S.; Heppeler, A.; Schmitt, J.S.; Mäcke H.R. *Eur. J. Nucl. Med.*, **2000**, *27*, 273.

[30] Maina, T.; Nock, B.; Nikolopoulou, A.; Sotiriou, P.; Loudos, G.; Maintas, D.; Cordopatis, P.; Chiotellis, E. *Eur. J. Nucl. Med. Mol. Imaging*, **2002,** *29,* 742.

[31] Decristoforo, C.; Maina, T.; Nock, B.; Gabriel, M.; Cordopatis, P.; Moncayo, R. *Eur. J. Nucl. Med. Mol. Imaging*, **2003,** *30*, 1211.

[32] Gabriel, M.; Decristoforo, C.; Maina, T.; Nock, B.; von Guggenberg, E.; Cordopatis, P.; Moncayo, R. *Cancer Biother. Radiopharm*., **2004,** *19,* 73.

[33] Barlos, K.; Gatos, D.; Kallitsis, J.; Papaphotiou, G.; Sotiriou, P.; Wenquing, Y.; Shafer, W. *Tetrahedron Lett*., **1989,** *30,* 3943.

[34] Carpino, L.A.; Han, G.Y. *J. Org. Chem*., **1972,** *37,* 3404.

[35] Piantini, U.; Sorensen, O.W.; Ernst, R.R. *J. Am. Chem. Soc*., **1982,** *104,* 6800.

[36] Bax, A.; Davis, D.G. *J. Magn. Reson*., **1985,** *65,* 355.

[37] Marion, D.; Wüthrich, K. *Biochem. Biophys. Res. Commun*., **1983,** *113,* 967.

[38] Jeener, J.; Meier, B.H.; Bachmann, P.; Ernst R.R. *J. Chem. Phys*., **1979,** *71,* 4546.

[39] Macura, S.; Wüthrich, K.; Ernst, R.R. *J. Magn. Reson*., **1982,** *47,* 351.

[40] Eccles, C.; Güntert, P.; Billeter, M.; Wüthrich, K. *J. Biomol. NMR*, **1991,** *1,* 111.

[41] Güntert, P.; Braun, W.; Wüthrich, K. *J. Mol. Biol*., **1991,** *217,* 517.

[42] Güntert, P.; Mumenthaler, C.; Wüthrich, K. *J. Mol. Biol*., **1997,** *273*, 283.

[43] Pearlman, D.A.; Case, D.A.; Caldwell, J.W.; Ross, W.S.; Cheatham, T.E.; Ferguson, D.M.; Seibel, G.L.; Singh, U.C.; Weiner, P.K.; Kollman, P.A. *AMBER 5.0*. University of California, San Francisco, **1997**.

[44] Pearlman, D.A.; Case, D.A.; Caldwell, G.C.; Siebel, G.L.; Singh, U.C.; Weiner, P.; Kollman, P.A. *AMBER 4.0*. University of California, San Francisco, **1991**.

[45] Koradi, R.; Billeter, M.; Wüthrich, K. *J. Mol. Graph*., **1996,** *14,* 51.

[46] Pohl, E.; Heine, A.; Sheldrick, G.M.; Dauter, Z.; Wilson, K.S.; Kallen, J.; Huber, W.; Pfaffli, P.J. *Acta Crystallogr*., **1995,** *D51,* 48.

[47] Wynants, C.; Van Binst, G.; Loosli, H.R. *Int. J. Pept. Protein Res*., **1985,** *25,* 608.

[48] Wynants, C.; Van Binst, G.; Loosli, H.R. *Int. J. Pept. Protein Res*., **1985,** *25,* 615.

[49] Wynants, C.; Tourwe, D.; Kazmierski, W.; Hruby, V.J.; Van Binst, G. *Eur. J. Biochem*., **1989,** *185,* 371.

[50] Maina, T.; Nikolopoulou, A.; Nock, B.; Tsipra, C.; Sotiriou, P.; Magafa, V.; Maindas, D.; Cordopatis, P.; Chiotellis, E. *Eur. J. Nucl. Med*., **2001,** *28*, S1022, OS_235.

[51] Nikolopoulou, A.; Nock, B.A.; Galanis, A.; Cordopatis, P.; Maina, T. *Eur. J. Nucl. Med. Mol. Imaging,* **2004,** *30,* S379, P414.

Received: 16 February, 2005 Accepted: 26 May, 2005